Metamorphic evolution of high-pressure Quartz Schists in the Chadegan metamorphic complex, Sanandaj-Sirjan zone, Iran

Javad Izadyar *, Moustafa Mousavizadeh, Mozafar Eram

Department of Geology, University of Zanjan, University Blvd., Zanjan, Iran
*Corresponding author, e-mail: izadyar@znu.ac.ir

Abstract

The Chadegan metamorphic complex is a WNW-ESE- trending antiformal structure located in Sanandaj-Sirjan structural zone, Iran. The inner core of the structure is made of orthogneiss, containing eclogitic lenses. Schists and marbles lie structurally above the orthogneiss and crop out in the external limbs of the antiformal dome. Two main deformational episodes have been documented in the schists and marbles. The first episode (D1 phase) produced S1 foliation, whereas the second episode (D2 phase) produced a penetrative S2 axial plane foliation, F2 folds, and a mylonitic fabric. Relicts of a high-pressure metamorphic mineral assemblage (M1) (phengite+ garnet + sodic-calcic amphibole) have been documented along S1 foliation. A later amphibolite-facies metamorphism (M2) occurred during D2 deformation phase. P-T estimates for M1 stage give an average pressure of 1.6 GPa and an average temperature of 550 °C, whereas M2 stage has been constrained at P = 0.34 – 0.48 GPa and T = 508 - 575 °C. D1 deformation phase and the associated high-pressure metamorphic assemblage (M1 stage), documented in the Chadegan complex, were formed during the subduction stage, while the D2 deformation phase and M2 metamorphic blastesis were recorded during the exhumation stage; probably they occurred before the end of Cretaceous.

Keywords: *Chadegan metamorphic complex, High-pressure quartz schist, Iran , P-T path, Sanandaj-Sirjan zone.*

Introduction

Iran has one of the largest tectonic provinces in southwestern Asia, and it is classically interpreted as a complicated puzzle, which originated after the collision between Eurasia and several Gondwana-derived continental fragments. These fragments are presently separated by discontinuous ophiolitic belts (Stöcklin, 1968; Berberian & King, 1981). Among these continental fragments, the Sanandaj-Sirjan zone (Stöcklin, 1968) is located between the central Iran block or microplate, in the east, and the Zagros fold-thrust belt_ located on northeastern margin of the Arabian platform_ on the west (Stöcklin, 1968; Alavi, 1994; Berberian, 1995; Ghasemi & Talbot, 2006) (Fig. 1). The Sanandaj-Sirjan zone stretches for 1500 km from northwest to southeast of Iran and is up to 200 km wide (Berberian, 1977; Mohajjel *et al*., 2003). It is divided into the "outer belt", made by imbricate thrust slices (e.g. the Zagros suture), and the "inner belt", made mainly by Mesozoic metamorphic rocks (Mohajjel *et al*., 2003). The Sanandaj-Sirjan zone records amphibolite-facies metamorphic assemblage acquired during the Cretaceous-Tertiary continental collision between the Arabian and Iranian continental plates (Şengör & Natal῾in, 1996; Mohajjel *et al*., 2003).

Recently, in north of Shahrekord city, in the central part of the Sanandaj-Sirjan zone, Davoudian

et al. (2008) documented for the first time, metro-to decameter-thick eclogitic lenses and orthogneiss, recording a high-pressure metamorphic event and a ductile mylonitic fabric trending parallel to the main Zagros reverse fault. Most of eclogitic lenses, recording pressure of 2.1-2.4 GPa, are retrogressed to garnet-amphibolite and/or amphibolite. Davoudian *et al*. (2008) also stated that quartz schists, amphibole schists and marbles surrounding the orthogneiss, and the eclogitic lenses are neither affected by high-pressure metamorphism nor by mylonitic deformation.

The different metamorphic conditions documented between orthogneiss (and eclogites) and the surrounding rocks can be explained either by assuming that the surrounding rocks have never reached high-pressure conditions (i.e. they are tectonically coupled with orthogneiss during the retrograde exhumation path) or assuming that they were buried together with orthogneiss, their high-pressure metamorphic assemblage is completely replaced during the retrograde amphibolites-facies event (e.g. Carswell *et al.,* 2000; Palmieri *et al.,* 2003).

To solve this question, we focused on quartz schists, the most abundant rocks surrounding the orthogneiss. To figure out if they have been coupled with the orthogneiss during the burial stage, we carried out detailed investigations on their

geometric field relationship, microstructure analyses, mineral chemistry, and thermobaric evolution.

Geological Framework

From the southwest to the northeast, the Sanandaj-Sirjan zone consists of several elongated sub-zones: (1) the Radiolarite sub-zone made of Triassic-Cretaceous shallow marine limestone and dominant deep-marine radiolarite; (2) the Bisotun sub-zone that includes Late Triassic to Late Cretaceous limestone; (3) the Ophiolite sub-zone that represents the Zagros suture zone; (4) the Marginal sub-zone that contains abundant Late Jurassic-Early Cretaceous volcanic rocks coupled with shallow marine deposits belonging to the Cretaceous unit; and (5) the Complexly deformed sub-zone, characterized by abundant schist, marble, amphibolite, quartzite, dolomite-marble and metasandstone (Mohajjel *et al.*, 2003) (Fig. 1). The Complexly deformed sub-zone was affected by a main Late Cretaceous deformation event that produced the northwest to west-northwest trending axial folds, faults, and foliation (Mohajjel *et al.*, 2003).
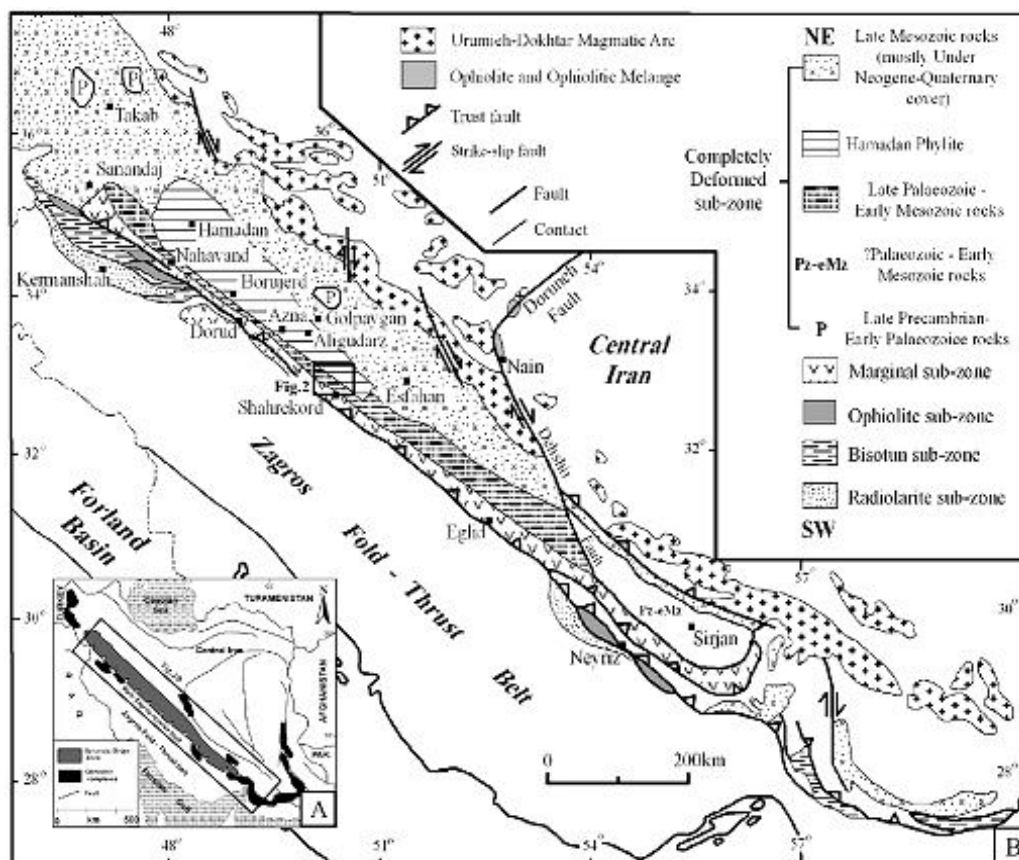

Figure 1: (A) Simplified geological map of Iran and location of Fig. 1B. (B) Simplified tectonic map of the Sanandaj-Sirjan zone (modified after Mohajjel *et al.*, 2003) (see Fig.1A for location).

All sub-zones are imbricated in a complicate thrust system, with out-of-sequence thrusts that locally juxtaposes younger units over older ones. Major thrusting has affected Miocene marine rocks and involved Neogene conglomerate. Locally, allochthons of the Bisotun sub-zone and Marginal sub-zone have been thrust toward the southwest, above the Zagros fold-and-thrust belt during Late Tertiary compressive tectonics (Mohajjel *et al.*, 2003).

The Chadegan metamorphic complex, located in the Sanandaj-Sirjan structural zone (Complexly deformed sub-zone, SW Iran), is close to the main Zagros reverse fault, which is classically interpreted as a suture zone between the Arabian plate and Eurasia (Şengör, 1984; Agard *et al.*, 2006; Ghasemi & Talbot, 2006)(Figs. 1 and 2).

Field investigations highlighted that the core of the complex is made of orthogneiss, containing several meter-thick eclogitic lenses. Amphibole

schists, quartz schists, marbles, and amphibolites, recording a polyphase tectono-metamorphic evolution, lie structurally above the orthogneiss and

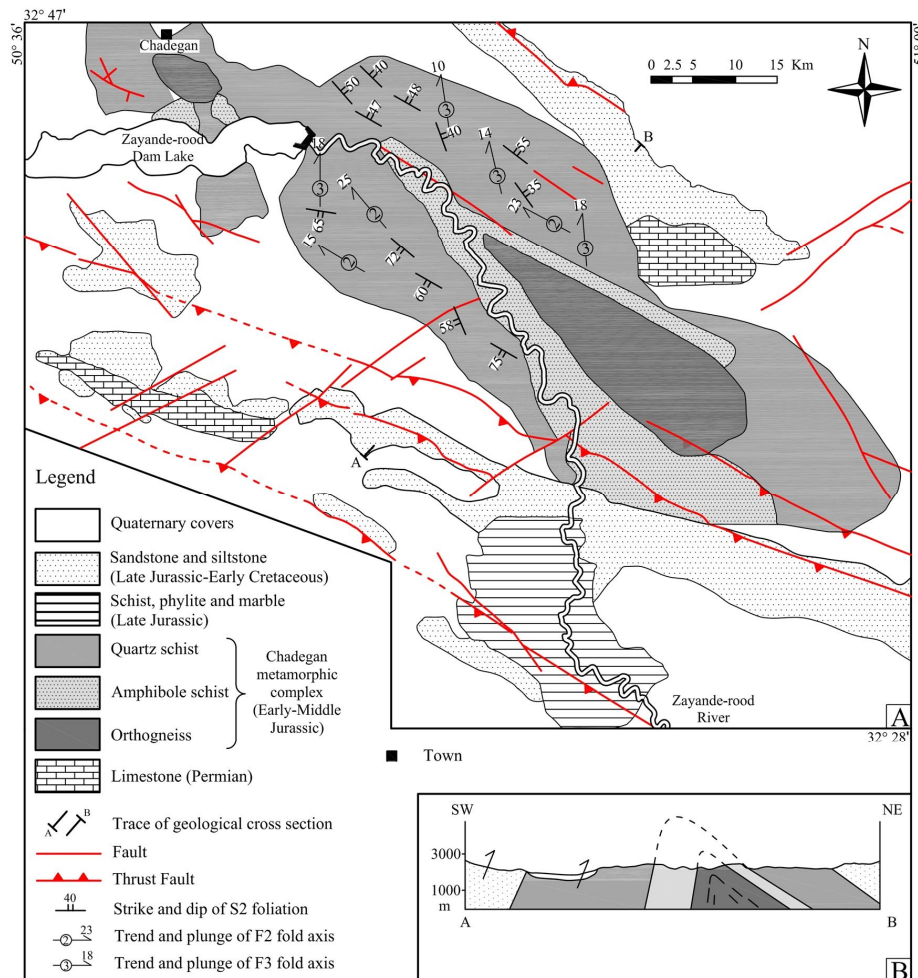crop out in the external limbs of the antiformal dome (Fig. 2).

Figure 2: (A) Geological sketch map of the Chadegan metamorphic complex, north of Shaherkord city (modified after Davoudian *et al.*, 2008). (B) Geological cross-section. For location on the map see Fig.2A.

The age of the rocks cropping out in the core and in the limbs of the Chadegan complex have been considered to be Early-Middle Jurassic because of the presence of late Jurassic-Early Cretaceous sandstone and siltstone cropping out on both limbs of the dome (Ghasemi *et al.*, 2005).

A km-thick ductile shear zone, highlighted by a penetrative mylonitic foliation and showing a WNW-ESE trend nearly parallel to the Chadegan antiformal axes, is described mainly in the orthogneiss.

Deformation and Petrography
Rocks of the inner core and the external limbs of the Chadegan complex recorded a polyphase tectono-metamorphic evolution.

D1 fabric is overprinted, and locally completely

transposed, by the main regional deformation phase documented in the area (D2 phase). D2 phase produced F2 folds, visible both at outcrop and microscopic scale, and a penetrative S2 foliation developed heterogeneously both as axial plane foliation and as mylonitic foliation.

F2 fold and S2 axial plane foliation were mainly recorded in quartz schist. F2 fold axes trends range from NW-SE to W-E with 15-20° plunge towards W-NW (Figs. 3A, 4A, 4B, 4C). Mylonitic fabric has been described mainly in the orthogneiss. In the quartz schists cropping out in the limbs of the Chadegan antiform, Mylonitic fabric is developed weakly and marked by σ-type albite porphyroclasts, asymmetrical pressure shadows, and elongated albite and quartz grains. S2 mylonitic foliation is parallel to both the S2 axial plane foliation (Figs.

4C, 4D) and to the boundary between quartz schists, amphibole schists, and orthogneiss on both limbs of the metamorphic dome. Evidence of motion along the shear planes with identical shears_ documented by σ-type albite porphyroclasts with asymmetrical trails_ was found on both limbs of the Chadegan antiformal dome. D1 and D2 structures

were deformed by a third deformation phase (D3) that produced S3 crenulation cleavage, F3 folds with NW-SE axis trending, and 10-15° plunging toward NW (Figs. 3B, 4E, 4F). No metamorphic growth or recrystallizations have been documented during D3 deformation phase.
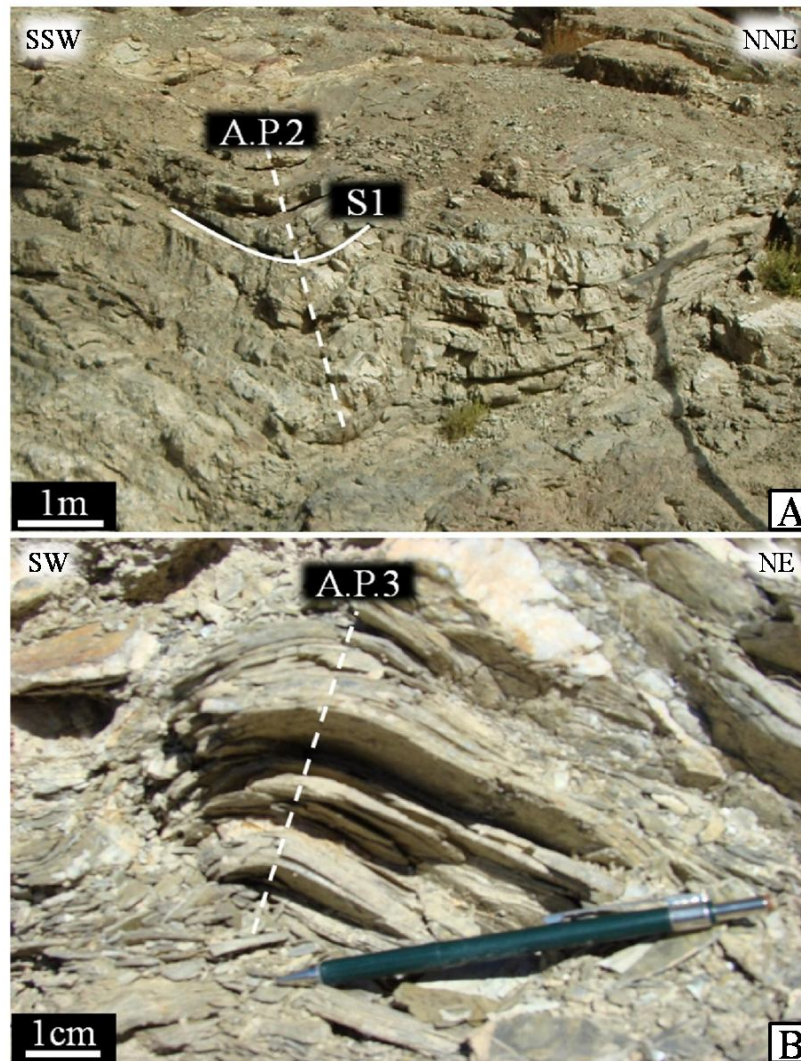

Figure 3: (A) Open F2 fold in quartz schist. S1: foliation of S1; A.P.2: axial plane of F2 fold. (B) F3 folds in quartz schist. A.P.3: axial planes of F3 folds.

The quartz schist consists of quartz, garnet, white mica, albite, amphibole, and chlorite with minor amounts of rutile, titanite, and rare alkali feldspar (Table 1). Inclusion trails in albite porphyroclasts are frequent and testify different episodes of metamorphic growth (Fig. 5D). Phengite, garnet, and sodic-calcic amphibole, preserved in albite core, are aligned along S1 foliation (Figs. 5A, 5B).

They have developed during D1 deformation phase, while garnet, calcic amphibole, and muscovite_ enveloped in the albite rim_ are oriented parallel to S2 foliation (Fig. 5B), reflecting the second metamorphic growth during D2 deformation. The S2 schistosity is defined by the alignment of fine-grained muscovite, chlorite, calcic, amphibole, elongated albite, and quartz grains (Fig. 5E).

Table 1: Mineral assemblages of quartz schists in the Chadegan metamorphic complex

Sample/Mineral	Qz	Ab	Ms	Ph(Inc)	Chl	Amp(Mat)	Amp(Inc)	Grt(Mat)	Afs	Spn
CH27	x	x	x	o	x	x	o	x	o	0
CH21	x	x	x	o	x	x	o	-	-	0
CH20	x	x	x	o	x	x	o	-	o	0
CH22	x	o	x	-	x	o	-	-	x	0
CH23	x	x	x	o	x	o	-	o	-	0

x, Major mineral; o, Minor mineral; Inc, Inclusion; Mat, Matrix. Mineral abbreviations after Whitney and Evans (2010)
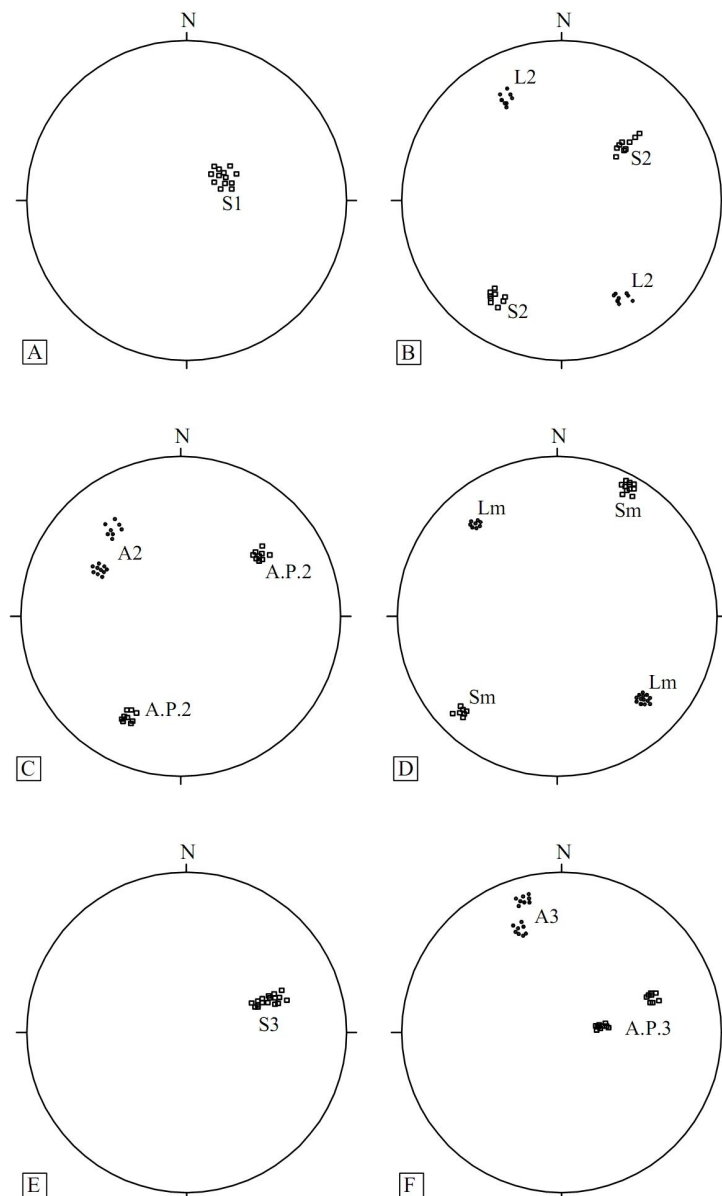

Figure 4: Equal area projections of main structural elements (lower hemisphere). (A) D1 deformation phase. S1: pole of foliation. (B) and (C) D2 deformation phase. L2: mineral lineation; S2: pole of foliation; A2: axes of F2 folds; A.P.2: pole of F2 folds axial planes. (D) Mylonitic fabric. Lm: mineral lineation; Sm: pole of mylonitic foliation. (E) and (F) D3 deformation phase. S3: pole of foliation; A3: axes of F3 folds; A.P.3: pole of F3 folds axial planes.
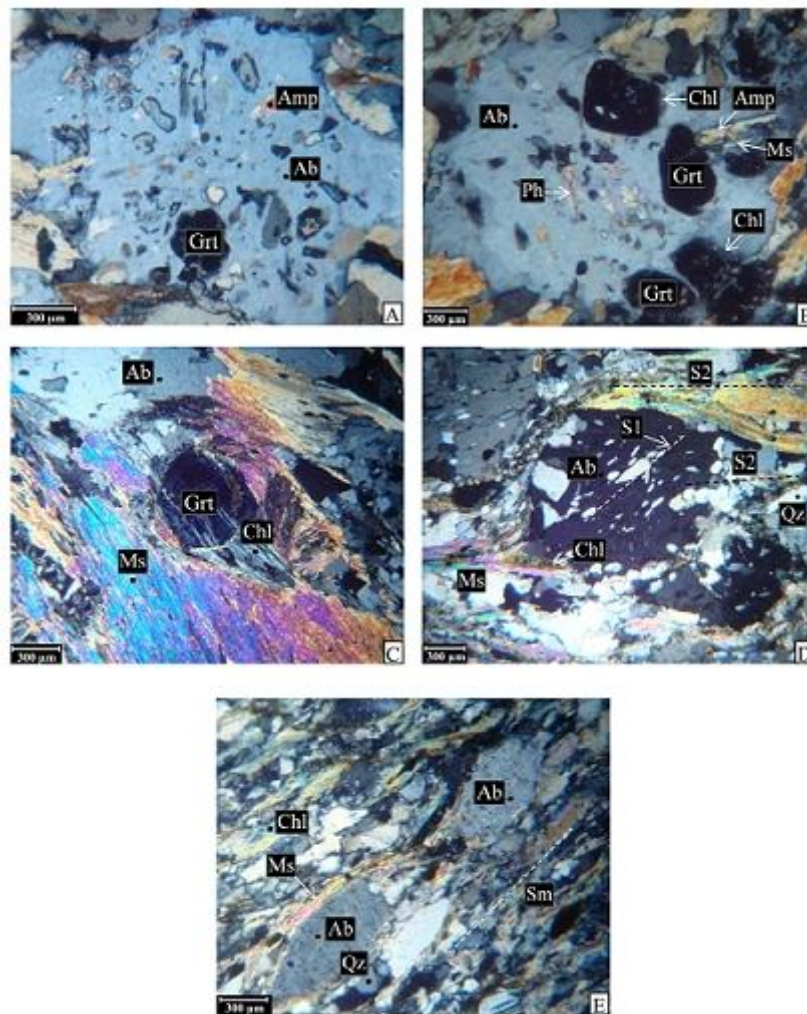
Figure 5: Photomicrographs of quartz schists from Chadegan metamorphic complex. (A) Garnet (Grt) and sodic-calcic amphibole (Amp) in the core of albite porphyroblast (Ab). (cross-polarized light). (B) Garnet (Grt), muscovite (Ms) and amphibole (Amp) included in the rim of albite porphyroblast (Ab). Garnet shows resorbed margins surrounded by chlorite (Chl). Phengite (Ph) is in the core of albite porphyroblast (Ab) (cross-polarized light). (C) Chlorite crystals (Chl) grew in pressure shadow of garnet porphyroclast (Grt) (cross-polarized light). (D) Inclusion trails in albite porphyroblast (Ab) defines both S1 foliation and S2 foliation. Asymmetrical pressure shadows made by muscovite (Ms) and chlorite (Chl) grew along S2 foliation (cross-polarized light). (E) The mylonitic foliation (Sm) is made by muscovite (Ms), chlorite (Chl) and elongate albite (Ab) and quartz (Qz) grains (cross-polarized light). Mineral abbreviations after Whitney & Evans (2010).

Garnet in quartz schist shows three different microstructural features: (1) euhedral garnets in the matrix enveloped by S2 schistosity, showing resorbed margins surrounded by chlorite; (2) euhedral garnets in the core of albite porphyroblast, and (3) euhedral garnets within albite rim, showing resorbed margin surrounded by chlorite as being the same as the garnet that occurred in the matrix (Figs. 5A, 5B, 5C).

Three different occurrences of amphibole can be distinguished: 1) amphibole occurring in S2 schistosity, usually having sodic-calcic composition rimmed by calcic amphibole; (2) sodic-calcic amphibole, included in albite core without chemical zoning structure; and (3) sodic-calcic amphibole in albite rim with chemical zoning rimmed by calcic amphibole as described for matrix amphibole (Figs. 5A, 5B).

Four types of white micas can be identified: (1) white mica in the matrix or following the S2 schistosity; (2) white mica in the pressure shadow of albite porphyroblasts; (3) white mica included in albite core, and (4) white mica inclusion in the rim of albite porphyroblasts (Figs. 5B, 5D, 5E). White mica that occurs in pressure shadow has muscovite composition, while those that occurr in the core of albite porphyroblast show phengitic composition. White mica in the matrix or included in albite rim is usually muscovite in composition and coexists with chlorite and makes S2 schistosity; however,

sometimes it shows chemical zoning in which its core is phengite and is rimmed by muscovite. In addition, some of the white micas in the matrix are altered to chlorite.

Chlorites occur with three different structural relations: (1) chlorite in the S2 schistosity, which is one of the main constituent minerals; (2) in pressure shadow of albite porphyroblast, and (3) replacement after garnet and white mica (Figs. 5B, 5C, 5D, 5E).

Titanite occurs as large grains in the matrix in which some of them are surrounding rutile in the core. Alkali feldspar is rare and is present in the phyllosilicate-rich layers only.

Mineral Chemistry

Mineral chemistry in quartz schists was acquired using a Cameca SX 50 electron microprobe equipped with three wavelength spectrometers at Toronto University (Canada) and a Cameca SX 100 at Iran Mineral Processing Research Center. The accelerating voltage and the beam current were maintained at 15 kV and 10 nA, respectively.

Corrections were made using either the ZAF or Phi-Rho-Z method, following Armstrong (1988). The structural formulae, the Fe^{3+}-content and the end-member activities of the minerals were recalculated using the AX program of Holland & Powell (www.esc.com.ac.uk/pub/minp/AX). The mineral abbreviations are from Whitney and Evans (2010).

Garnet

Within the different microstructural domains, garnets show similar chemical compositions. They show: (1) almandine-rich composition, and (2) concentrically zoning with cores relatively richer in Mn and Ca and poorer in Fe^{2+} and Mg. For example, the garnet preserved in the matrix (i.e. along the S2 foliation) shows, from the core to the rim, an increase in pyrope and almandine components and a decrease in spessartine and grossular contents (core composition in %mole: $X_{Prp}=3$, $X_{Alm}=49$, $X_{Sps}=9$, $X_{Grs}=35$; rim composition in %mole: $X_{Prp}=10$, $X_{Alm}=55$, $X_{Sps}=2$, $X_{Grs}=30$) (Figures 6A, 6B and 6C) (Table 2).
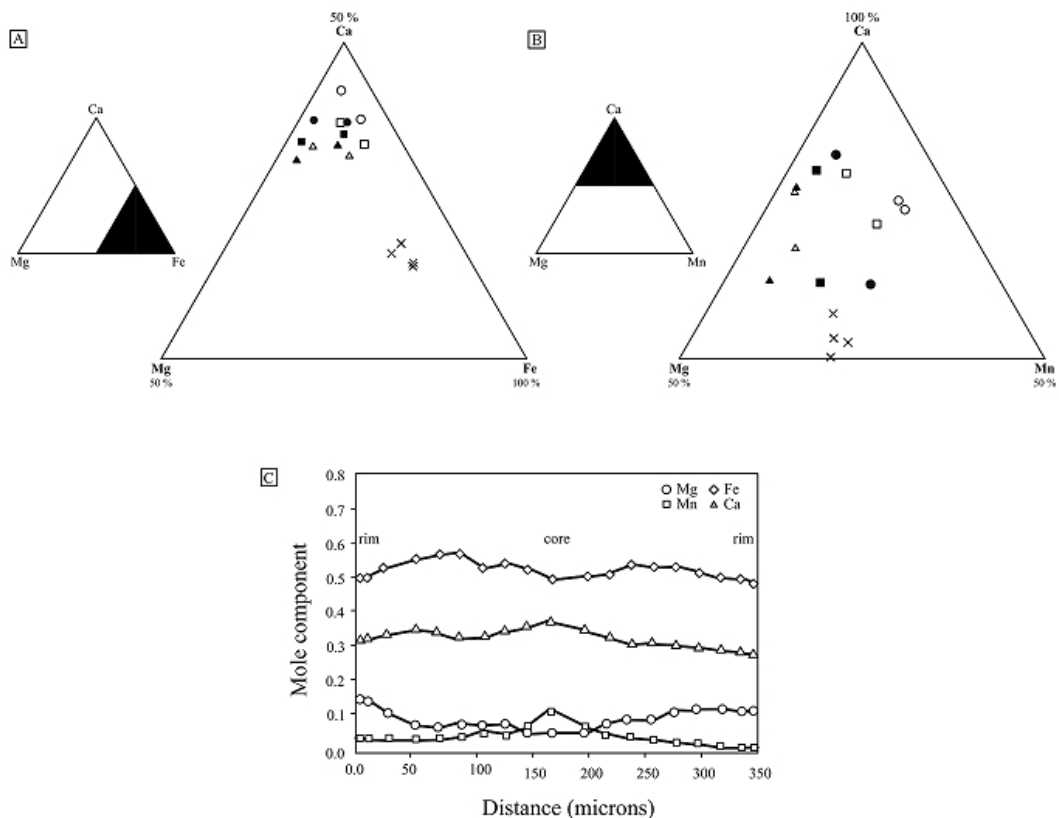

Figure 6: Garnet compositions plotted on Ca-Mg-Fe (A) and on Ca-Mg-Mn (B) diagrams. Filled symbols represent composition from garnet inclusions in albite porphyroblast, open symbols represent composition from garnet crystals embedded by S2 foliation. Circle, square and triangle symbols represent garnet composition obtained from core, mantle and rim sites respectively. Multiply symbol shows garnet composition in contact to chlorite. (C) Compositional profile across garnet grain in sample CH27.

Table 2: Representative microprobe analyses of garnet.

Rock	CH27														CH20			
Location	Matrix							Inclusion in albite							Contact with chlorite			
Point	M1	M2	M3		M11	M12	M13	I1	I2	I3		I11	I12	I13	-	-	-	-
Position	Core	Mantle	Rim		Core	Mantle	Rim	Core	Mantle	Rim		Core	Mantle	Rim	-	-	-	-
Wt% oxide																		
SiO$_2$	37.8	38	38		37	37.58	37.2	37.60	37.9	37.9		37.5	37.22	37.8	37.2	37.1	38.40	37.7
TiO$_2$	0.10	0.10	0.12		0.11	0.13	0.12	0.10	0.10	0.10		0.02	0.14	0.08	0.08	0.05	0.10	0.04
Al$_2$O$_3$	22.1	22.1	22.2		21.8	22.61	20.8	21.6	21.8	22.1		20.8	20.32	20.1	21.5	21.5	20.3	20.4
Fe$_2$O$_3$	0.00	0.00	0.00		1.72	1.03	3.97	1.64	1.04	0.37		3.10	4.27	3.52	0.00	0.67	0.00	0.45
FeO	22.9	26.1	26.9		21.3	23.37	23.1	24.9	25.4	25.1		21.6	21.47	23	32.1	31.9	30.2	31.2
MnO	3.96	1.43	0.52		4.37	3.54	1.50	1.15	0.85	0.32		4.72	3.01	1.31	2.39	2.60	3.08	2.30
MgO	0.87	1.26	2.12		0.92	1.45	3.02	1.41	1.83	3.26		2.31	3.12	3.86	1.85	1.83	2.44	1.94
CaO	13	11.3	10.9		13.2	12.06	11.2	12.8	12.3	10.8		11.2	11.01	10.7	4.93	4.89	5.37	6.02
Na$_2$O	0.00	0.02	0.03		0.01	0.00	0.02	0.01	0.00	0.05		0.00	0.07	0.05	0.02	0.07	0.03	0.06
K$_2$O	0.03	0.00	0.01		0.01	0.02	0.01	0.02	0.03	0.03		0.01	0.04	0.04	0.01	0.00	0.01	0.02
Total	101	100	101		####	101.8	101	####	101	100		101	100.7	100	100	101	99.9	100
Formula	12(O)	12(O)	12(O)		12(O)	12(O)	12(O)	12(O)	12(O)	12(O)		12(O)	12(O)	12(O)	12(O)	12(O)	12(O)	12(O)
Si	2.98	3.00	2.98		2.93	2.93	2.92	2.95	2.96	2.98		2.94	2.93	2.97	2.98	2.97	3.07	3.02
Ti	0.01	0.01	0.01		0.01	0.008	0.01	0.01	0.01	0.01		0	0.008	0.01	0.01	0	0.01	0
Al	2.05	2.05	2.05		2.03	2.07	1.92	2.00	2.01	2.04		1.93	1.89	1.86	2.03	2.02	1.91	1.93
Fe^{3+}	0.00	0.00	0.00		0.10	0.06	0.23	0.10	0.06	0.02		0.18	0.25	0.21	0.00	0.04	0.00	0.03
Fe^{2+}	1.50	1.72	1.76		1.41	1.52	1.52	1.63	1.66	1.65		1.42	1.41	1.51	2.15	2.15	2.02	2.10
Mn	0.26	0.10	0.03		0.29	0.23	0.10	0.07	0.05	0.02		0.31	0.20	0.09	0.16	0.18	0.21	0.16
Mg	0.10	0.15	0.25		0.11	0.17	0.35	0.16	0.21	0.38		0.27	0.37	0.45	0.22	0.21	0.29	0.23
Ca	1.09	0.96	0.92		1.12	1.00	0.94	1.07	1.03	0.90		0.94	0.93	0.90	0.42	0.42	0.46	0.52
Na	0.00	0	0.01		0	0.00	0	0	0.00	0.01		0.00	0.01	0.01	0	0.01	0.01	0.01
K	0	0.00	0		0	0.002	0	0	0	0		0	0.004	0	0	0.00	0	0
Total	7.99	7.99	8.00		8.00	7.99	7.99	7.99	7.99	8.00		7.99	8.00	8.00	7.99	8.00	7.98	8.00
X$_{Alm}$%	52	57	59		47	51	51	54	55	55		47	47	50	72	71	67	70
X$_{Prp}$%	3	5	8		4	8	13	5	7	13		9	13	15	8	7	10	8
X$_{Grs}$%	36	33	31		33	30	20	31	32	29		23	21	19	14	14	15	16
X$_{Sps}$%	8	4	1		10	8	4	3	1	1		11	6	3	6	6	7	5
X$_{And}$%	-	-	-		5	3	12	5	3	1		9	12	11	-	2	-	1

Mineral abbreviations after Whitney and Evans (2010). The structural formulae and the Fe^{3+}-iron recalculated with the AX program of Holland and Powell.

The same trend has been observed for the garnet included in albite porphyroblast (core composition in %mole: X$_{Prp}$=7, X$_{Alm}$=50, X$_{Sps}$=8, X$_{Grs}$=34; rim composition in %mole X$_{Pyr}$=12, X$_{Alm}$= 54, X$_{Sps}$=2, X$_{Grs}$=30) (Figs. 6A, 6B) (Table 2). The bell-shaped zoning of Mn and bowl-shaped zoning of Mg are

generally attributed to growth zoning during prograde metamorphism (e.g., Spear, 1991). However, the garnet located in the matrix, or preserved as inclusion in the rim of albite porphyroblast, is locally replaced by chlorite. In this case, closer to chlorite boundary, garnet becomes richer in Fe and Mn and poorer in Ca and relatively poorer in Mg (X_{Prp}=8, X_{Alm}=70, X_{Sps}=6, X_{Grs}=15) (Figs. 6A, 6B) (Table 2). This feature could be indicative of retrograde metamorphism.
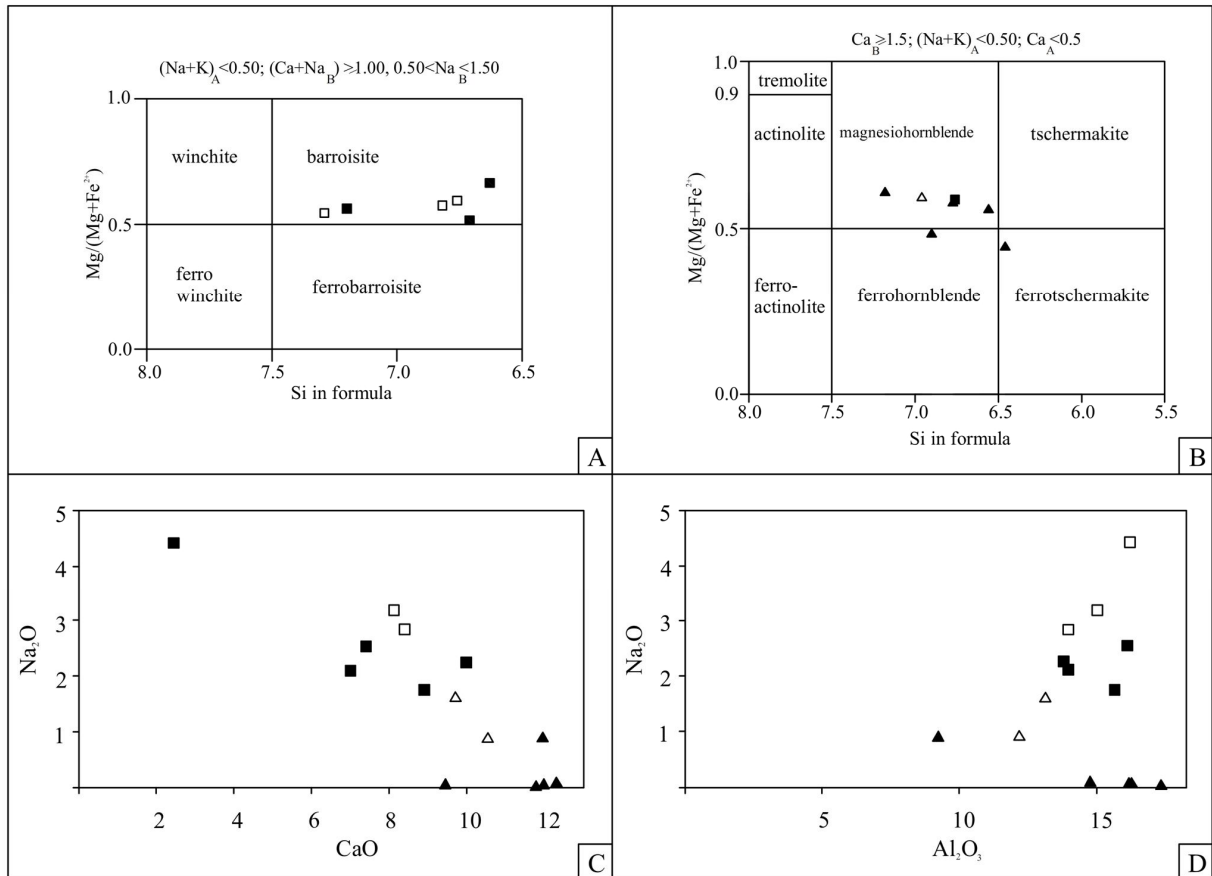

Figure 7: Composition diagrams for sodic-calcic (A) and calcic (B) amphiboles. (C) Na_2O *vs* CaO plot. (D) Na_2O *vs* Al_2O_3 plot. Triangle and square symbols represent compositions of rim and core respectively. Filled symbols show amphibole crystals grew along S2 foliation and open symbols, those included in albite porphyroblasts.

Amphibole

According to the IMA classification scheme (Leake *et al.,* 1997), we documented two main amphibole groups: (1) sodic-calcic amphiboles such as alumino-barroisite, and (2) calcic amphiboles such as ferrotschermakite, magnesiohornblende, alumino-magnesiohornblende, and ferrohornblende (Figs. 7A, 7B) (Table 3). Amphiboles grew along S2 schistosity and included albite porphyroblast rim, usually containing two chemical zoning. Their cores have alumino-barroisite composition, whereas their rims show magnesiohornblende composition in crystals_ including albite rims and a composition raging from ferrotschermakite, ferrohornblende and alumino-magnesiohornblende for those aligned along the S2 foliation. Amphiboles preserved within the core of albite blasts show a homogenous alumino-barroisite composition (Leake *et al.*, 1997) (Figs. 7A, 7B) (Table 3).

Our investigations on amphibole compositional zoning show that calcic amphibole grew exclusively as rim around sodic-calcic amphibole. This data indicates that the core grew close to, or during, the metamorphic peak conditions, whereas the rims developed during retrograde metamorphic condition was formed probably during the D2 deformation (Figures 7C, 7D). The term retrograde is normally used to describe a decrease in metamorphic temperature. On the other hand, zoning pattern of amphibole, discussed above, probably causes a decrease in pressure, since the calcic amphibole is a hornblende/tschermakite with relatively high Al-content.

Table 3: Representative microprobe analyses of amphibole.

Rock	CH27													
Location	Marix									Inclusion in albite				
Position	Core	Rim	Core	Rim	Core	Rim	Core	Rim	-	Core	Rim	Core	Rim	-
Wt% oxides														
SiO_2	46.56	43.74	46.4	48	46.3	49.3	50.9	45	47.3	46.65	44.72	46.9	48.5	51.7
TiO_2	0.42	0.31	0.41	0.51	0.48	0.22	0.35	0.31	0.31	0.61	0.29	0.72	0.61	0.02
Al_2O_3	15.65	17.34	16.1	16.2	13.80	9.22	14	16.2	14.7	13.97	13.15	15	12.2	16.2
Fe_2O_3	1.30	0.00	2.94	0.00	0.66	0.00	0.00	0.00	0.00	2.58	4.07	0.47	0.28	0.00
FeO	14.52	15.8	9.84	14.5	12.6	13.4	13.50	14.50	12.9	11.89	12.23	12.1	13.5	12.9
MnO	0.21	0.40	0.21	0.20	0.11	0.24	0.11	0.90	0.20	0.22	0.34	0.30	0.37	0.35
MgO	8.61	7.11	11	8.04	10.2	11.7	9.73	8.31	9.83	9.75	10.09	9.19	11	8.69
CaO	8.91	11.8	7.41	9.45	10.00	12	7.01	12.00	12.3	8.39	9.71	8.12	10.5	2.45
Na_2O	1.75	0.01	2.55	0.05	2.26	0.89	2.12	0.06	0.07	2.84	1.61	3.19	0.91	4.43
K_2O	0.46	0.39	0.62	0.62	0.65	0.31	0.35	0.65	0.34	0.52	0.77	0.69	0.43	0.12
Total	98.39	96.90	97.5	97.6	97.1	97.3	98.00	97.90	98	97.42	96.98	96.7	98.3	####
Formula	23(O)	23(O)	23(O)	23(O)	23(O)	23(O)	23(O)	23(O)	23(O)	23(O)	23(O)	23(O)	23(O)	23(O)
Si	6.71	6.46	6.63	6.90	6.76	7.18	7.20	6.56	6.77	6.76	6.60	6.82	6.96	7.29
Ti	0.05	0.03	0.04	0.05	0.05	0.02	0.04	0.03	0.03	0.07	0.03	0.08	0.07	0
Al	2.66	3.02	2.72	2.75	2.37	1.58	2.33	2.79	2.50	2.39	2.29	2.57	2.07	2.69
Fe^{3+}	0.14	0.00	0.32	0.00	0.07	0.00	0.00	0.00	0.00	0.28	0.45	0.05	0.03	0.00
Fe^{2+}	1.75	1.95	1.18	1.84	1.53	1.64	1.60	1.77	1.55	1.44	1.51	1.47	1.62	1.54
Mn	0.03	0.05	0.02	0.02	0.01	0.03	0.01	0.11	0.02	0.03	0.04	0.04	0.04	0.04
Mg	1.85	1.56	2.35	1.72	2.21	2.53	2.05	1.81	2.10	2.11	2.22	1.99	2.36	1.84
Ca	1.38	1.87	1.13	1.50	1.56	1.87	1.06	1.88	1.90	1.30	1.54	1.26	1.61	0.37
Na	0.49	0.003	0.69	0.01	0.64	0.25	0.58	0.02	0.02	0.80	0.46	0.89	0.25	1.21
K	0.08	0.07	0.11	0.11	0.12	0.06	0.06	0.12	0.06	0.09	0.14	0.13	0.08	0.02
Total	15.14	15.01	15.2	15	15.3	15.2	15	15.1	15	15.27	15.28	15.30	15.1	15

The structural formulae of minerals and the Fe^{3+}-iron recaculated with the AX program of Holland and Powell.

White mica

White mica along with S2 schistosity usually shows two chemical zoning in which the core deviates from ideal muscovite end-member composition toward celadonite, by tschermak substitution ($MgSi=Al_{-1}Al_{-1}$) and toward Fe-celadonite, by the $Mg=Fe^{+2}$ substitution (core composition in %mole: $X_{Ms}=14$, $X_{Cel}=62$, $X_{Fcel}=22$) (Fig. 8) (Table 4). White mica rim, however, is close to ideal muscovite end-member (rim composition in %mole: $X_{Ms}=67$, $X_{Cel}=20$, $X_{FCel}=10$) (Fig. 8) (Table 4). White micas preserved as inclusions in the core of albite show a homogeneous composition that deviates from ideal muscovite end-member by $MgSi=Al_{-1}Al_{-1}$ and $Mg=Fe^{+2}$ substitutions (composition in %mole: $X_{Ms}=14$, $X_{Cel}=64$, $X_{Fcel}=16$) (Fig. 8) (Table 4). We documented a phengitic composition in white mica preserved in the cores of albite crystals and a composition close to the ideal muscovite end-member preserved at albite rims. White mica in pressure shadow shows chemical composition close to the ideal muscovite (composition in %mole: $X_{Ms}=71$, $X_{Cel}=17$, $X_{Fcel}=10$) (Fig. 8) (Table 4).

It is well known that an enrichment of celadonite component indicates an increase of pressure (Deer *et al.,* 1992). Therefore, a decrease in celadonite component_ documented from the core towards the

rim in white micas laying along the S2 schistosity_ indicates that their growth occurred during a decompressive path in which the D2 deformation phase occurred during the lowest pressure condition.

Table 4: Representative microprobe analyses of white mica

Rock	CH21													
Location	Marix								Inclusion in albite			Pressure Shadow		
Position	Core	Rim	Core	Rim	Core	Rim	-	-	-	-	-	-	-	-
Wt% oxides														
SiO_2	51.62	48.1	50.12	47.7	51.3	48.1	47.3	47.6	51.81	50.9	51.4	47.5	47.1	47.9
TiO_2	0.30	0.50	0.20	0.40	0.40	0.20	0.58	0.90	0.29	0.12	0.23	0.71	0.12	0.02
Al_2O_3	20.65	34.1	21.22	31.7	20.9	32.2	35.1	33.2	21.47	22	22.4	33.4	32.2	34.1
Fe_2O_3	3.84	1.24	4.76	2.88	4.61	1.73	1.79	1.10	2.33	3.98	3.21	1.67	2.43	1.87
FeO	1.48	0.74	1.84	1.11	1.78	0.67	0.69	0.42	0.90	1.54	1.24	0.65	0.94	0.72
MnO	0.05	0.00	0.05	0.00	0.01	0.03	0.02	0.01	0.04	0.06	0.02	0.01	0.01	0.03
MgO	6.14	1.53	7.21	1.70	7.73	2.99	1.04	2.32	6.23	5.53	7.77	1.61	1.76	1.83
CaO	0.00	0.01	0.00	0.00	0.00	0.02	0.00	0.02	0.00	0.02	0.00	0.01	0.00	0.03
Na_2O	0.27	0.30	0.31	0.30	0.30	0.20	0.32	0.22	0.21	0.12	0.12	0.30	0.40	0.20
K_2O	10.20	9.95	9.82	9.91	9.78	10	9.78	10.10	10.42	10.3	9.98	9.80	10.1	10.10
Total	94.55	96.5	95.53	95.7	96.8	96.2	96.6	95.8	93.70	94.60	96.3	95.7	95.1	96.9
Formula	O(11)	O(11)	O(11)	O(11)	O(11)	O(11)	O(11)	O(11)	O(11)	O(11)	O(11)	O(11)	O(11)	O(11)
Si	3.51	3.14	3.39	3.17	3.42	3.17	3.10	3.13	3.53	3.46	3.42	3.14	3.15	3.13
Ti	0.015	0.02	0.01	0.02	0.02	0.01	0.03	0.04	0.01	0.01	0.01	0.03	0.01	0
Al	1.65	2.63	1.69	2.48	1.64	2.50	2.70	2.58	1.72	1.77	1.75	2.62	2.54	2.63
Fe^{3+}	0.20	0.06	0.24	0.14	0.23	0.08	0.09	0.05	0.12	0.20	0.15	0.08	0.12	0.09
Fe^{2+}	0.08	0.04	0.10	0.06	0.10	0.04	0.04	0.02	0.05	0.09	0.07	0.04	0.05	0.04
Mn	0.003	0.00	0.003	0.00	0	0	0	0	0.002	0	0	0	0	0
Mg	0.62	0.15	0.73	0.17	0.77	0.29	0.10	0.23	0.63	0.56	0.77	0.16	0.17	0.18
Ca	0.001	0	0.00	0.00	0.00	0	0.00	0	0.00	0	0.00	0	0.00	0
Na	0.04	0.04	0.04	0.04	0.04	0.03	0.04	0.03	0.03	0.02	0.01	0.04	0.05	0.02
K	0.89	0.83	0.85	0.84	0.83	0.84	0.82	0.85	0.90	0.89	0.85	0.83	0.86	0.84
Total	7.01	6.91	7.05	6.92	7.05	6.96	6.92	6.93	6.99	7.00	7.03	6.94	6.95	6.93
X_{Ms} %	12	78	11	67	10	64	80	72	12	21	9	73	69	70
X_{Cel} %	62	15	62	17	63	29	10	23	63	56	74	16	17	18
X_{Fcel} %	20	6	24	14	23	9	8	5	12	2	15	8	12	9

Mineral abbreviations after Whitney and Evans (2010). The structural formulae and the Fe^{3+}-iron recalculated with the AX program of Holland and Powell

Chlorite

Chlorite composition deviates from ideal clinochlore end-member towards amesite by tschermak substitution ($MgSi=Al_{-1}Al_{-1}$), towards daphnite by $Fe^{+2}=Mg$ substitution, and towards sudoite by di/trioctahedral substitutions [$(Mg,Fe^{+2})_3=\square Al_{-2}$]. Comparing chemical compositions of chlorites laying along the S2 schistosity, chlorites grew in the pressure shadow of albite porphyroblasts, and chlorites grew as a reaction of instable garnets, emerges that chlorite grew on garnets contains relatively more clinochlore and daphnite and less amesite end-members compared to the others (Table 5).

Table 5: Representative microprobe analyses of chlorite

Rock	CH21	CH20		CH21	
Location	Matrix	After garnet	After mica	Pressure shadow	
Wt% oxides					
SiO$_2$	26.6	28.39	26.33	29.24	29.68
TiO$_2$	0.02	0.00	0.05	0.05	0.22
Al$_2$O$_3$	18.16	18.64	18.56	18.29	18.30
FeO	28.06	26.82	28.86	25.91	25.21
MnO	0.23	0.17	0.37	0.11	0.21
MgO	11.43	11.17	11.20	11.80	12.42
CaO	0.07	0.16	0.09	0.10	0.12
Na$_2$O	0.15	0.18	0.09	0.12	0.03
K$_2$O	0.10	0.32	0.14	0.16	0.85
Total	84.82	85.85	85.69	85.78	87.04
Formula	O(14)	O(14)	O(14)	O(14)	O(14)
Si	2.95	3.07	2.90	3.14	3.13
Ti	0.002	0.00	0.004	0.004	0.02
Al	2.37	2.37	2.41	2.31	2.28
Fe^{2+}	2.60	2.42	2.66	2.32	2.23
Mn	0.02	0.01	0.03	0.01	0.02
Mg	1.89	1.80	1.84	1.87	1.95
Ca	0.008	0.02	0.01	0.01	0.01
Na	0.03	0.04	0.02	0.02	0.006
K	0.01	0.04	0.02	0.02	0.11
Total	9.88	9.77	9.89	9.70	9.76

The structural formulae recalculated with the AX program of Holland and Powell

Metamorphism and P-T Conditions

Microstructural investigations and mineral chemistry results indicate that quartz schists in the Chadegan complex record two events of metamorphism. The older event (M1) is testified by relicts of high-pressure metamorphic mineral assemblage (i.e. phengite + garnet + sodic-calcic amphibole), preserved along S1 foliation in the core of albite, which had developed during the D1 deformation phase. On the other hand, a later amphibolite-facies metamorphism (M2 event), documented to have calcic amphibole, muscovite, and chlorite aligned along the S2 schistosity, occurred during D2 deformation phase (Table 6).

In order to constrain the P and T conditions recorded by the quartz schists during M1 and M2 metamorphic events, we defined the microstructural domains where mineral assemblages are close to metamorphic equilibrium. Then to obtain a solid and robust dataset, we applied different thermodynamic methods. To estimate P and T representative for each metamorphic phase, we used the mean mineral compositions. With garnets, however, a different approach was necessary because they generally preserve prograde zoning (i.e. increase in Mg content moving toward the rim) and evidence of retrograde resorption. For this reason, to estimate the metamorphic conditions higher pressure (M1 event), we used the least resorbed garnets that preserve rims with higher Mg content. For the amphibolite-facies metamorphism (M2), however, the resorbed rim composition was used (Table 6).

Table 6. The stability periods for minerals in quartz schists and the relationship between metamorphism, mineral crystallization, mineral composition and deformation phases in the Chadegan metamorphic complex. Abbreviations for mineral names are from Whitney and Evans (2010).

Mineral name	Defomation phases and Metamorohic stages		Microstructural domain	Mineral composition
	M1 (D1)	**M2 (D2)**		
Garnet	----------------------		Main schistosity (matrix)	X_{Prp}=10, X_{Alm}=55, X_{Grs}=30, X_{Sps}=2
Garnet	----------------------		Core of albite porphyroblast	X_{Prp}=12, X_{Alm}=54, X_{Grs}=30, X_{Sps}=2
Garnet		------------------	Rsorbed in main schistosity (matrix)	X_{Prp}=8, X_{Alm}=70, X_{Grs}=15, X_{Sps}=6
White mica	----------------------		Core of white mica in main schistosity (matrix)	X_{Ms}=14, X_{Cel}=62, X_{Fcel}=22
White mica		------------------	Main schistosity (matrix)	X_{Ms}=67, X_{Cel}=20, X_{Fcel}=10
White mica	------------------		Core of albite porphyroblast	X_{Ms}=14, X_{Cel}=64, X_{Fcel}=16
White mica		------------------	Pressure shadow	X_{Ms}=71, X_{Cel}=17, X_{Fcel}=10
Chlorite		------------------	Main schistosity (matrix)	Clc+Dph+Sud
Chlorite			Pressure shadow	Clc+Dph+Sud
Chlorite		------------------	Replacement after garnet	Clc+Dph+Sud
Amphibole	------------------		Core of amphibole in main schistosity (matrix)	Brs
Amphibole		------------------	Main schistosity (matrix)	Ts+Mhb
Amphibole	------------------		Core of albite porphyroblast	Brs
Amphibole		------------------	Rim of albite porphyroblast	Mhb
Albite	------------------	------------------		
Quartz	----------------------	------------------		

For the amphibole and white mica with compositional zoning, the core compositions (i.e. sodic-calcic amphibole and phengite) were used to estimate the P-T conditions of M1 metamorphic event while their rim compositions (i.e. calcic amphibole and muscovite) were utilized for P-T estimates on the amphibolite-facies metamorphism (M2 event) (Table 6).

Thermobarometry on M1 and M2 metamorphic events was mostly performed using calibrated geothermobarometers and the THERMOCALC 3.26 program (Powell & Holland, 1988) in average PT mode with the self-consistent thermodynamic dataset of Holland & Powell (1998).

Temperature of M1 metamorphic event was estimated using different calibrations of geothermometers based on the Fe-Mg partitioning between garnet and phengite (Krogh & Raheim, 1978; Green & Hellman, 1982) and between garnet and amphibole (Ravna, 2000). Assuming P =1.65 GPa, temperature estimates for mineral assemblage preserved in the core of albite porphyroblasts range from 447 ºC (for garnet-amphibole) to 493-532 ºC (for garnet-phengite), whereas temperature estimates
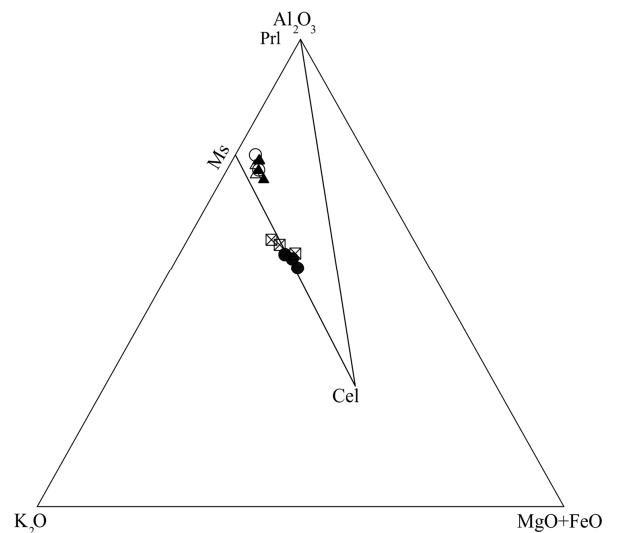
Figure 8. White mica compositions, plotted on Al_2O_3 - K_2O - MgO + FeO diagram (adapted from Vidal & Parra, 2000). Core and rim compositions of white mica crystals grew along S2 foliation, are indicated by filled and open circles respectively. Filled triangles indicate composition of white mica crystals in pressure shadows. White squares show compositions of white mica inclusions in albite porphyroblast. Mineral abbreviations after Whitney & Evans (2010).

for M1 mineral assemblage presented by the core of

garnet, amphibole and white mica laying along S2 foliation yield temperatures from 472 ºC (for garnet-amphibole) to 512-560 ºC (for garnet-phengite) (Table 7).

Table 7: Estimated temperatures for M1 and M2 metamorphic stages using different thermometers.

Metamorphic stages	Kinds of thermometers	Kinds of calibrations	LnK$_D$	T(˚C)
Peak metamorphic	Garnet-Phengite	Krogh and Raheim (1978)	3.96	512
stage of M1 using	Garnet-Phengite	Green and Helman (1982)	3.96	560
matrix assemblage	Garnet-amphibole	Ravna (2000)	2.04	472
Peak metamorphic	Garnet-Phengite	Krogh and Raheim (1978)	3.69	493
stage of M1 using	Garnet-Phengite	Green and Helman (1982)	3.69	532
inclusion assemblage	Garnet-Amphibole	Ravna (2000)	2.22	447
Post peak metamorphic	Garnet-Chlorite	Ghent *et al.*(1987)	-2	521
stage of M2	Garnet-Chlorite	Grambling (1990)	-2	523
	Amphibole-Plagioclase	Dale *et al.* (2000)	-2.88	508

The equation Ab = Jd + Qz can be used to constrain the pressure stability field for the M1 metamorphic assemblage. Since jadeite is absent in our rocks and albite coexists with quartz, we assumed a maximum pressure of 1.65 GPa (Holland, 1980) at nominal temperature of 550 °C for both M1 mineral assemblages occurring in the S2 schistosity and inclusions in the core of albite porphyroblast. Slightly different pressure estimates were obtained using the phengite barometer of Massonne & Schreyer (1987). Assuming Si = 3.5 and temperature of 550 ºC, in fact, we obtained a maximum pressure of 1.5 GPa.

The average P-T estimates obtained using THERMOCALC yield T = 580 ºC and P = 1.66 GPa for the M1 preserved in the core of albite porphyroblasts and T =565 ºC and P = 1.6 GPa for the M1 mineral assemblage preserved along S2 foliation (Table 8).

Table 8: Temperatures and pressures for M1 and M2 metamorphic stages caculated with THERMOCALC (Powell and Holland, 1988) with estimated uncertainities and sigfit parameters. End-member activities were calculated with the AX program of Holland and Powell (www.esc.com.ac.uk/minp/AX). Mineral name abbreviations are from Whiney and Evans (2010).

Metamorphic stage	Mineral assemblage	Activity	T(˚C) (sd)	P(GPa) (sd)	Sigfit
Peak metamorphic	Garnet, White mica,	Prp=0.0028, Grs=0.037, Alm=0.18			
stage of M1 using	Amphibole, Albite,	Ms=0.15, Cel=0.26, Pg=0.06	565 (36)	1.6 (0.15)	1.38
matrix assemblage	Quartz, H2O	Prg=0.158, Gln=0.03			
Peak metamorphic	Garnet, White mica,	Prp=0.0038,Grs=0.046, Alm=0.15			
stage of M1 using	Amphibole, Albite,	Ms=0.18, Cel=0.29, Pg=0.06	580 (67)	1.66 (0.12)	1.66
inclusion assemblage	Quartz, H2O	Prg=0.16, Gln=0.097, Fgl=0.055			
Post peak metamorphic	Garnet, White mica,	Prp=0.001,Grs=0.0037, Alm=0.35			
stage of M2	Amphibole, Chlorite,	Ms=0.58, Pa=0.30, Cel=0.046	575 (33)	0.34 (0.13)	1.96
	Albite, Quartz, H2O	Tr=0.03, Fact=0.013, Ts=0.023			
		Cln=0.01, Dph=0.055, Ame=0.0096			

Temperature of M2 metamorphic event was estimated using amphibole-plagioclase geothermometer (Dale *et al.*, 2000) and different calibrations of geothermometers based on the Fe-Mg partitioning between garnet-chlorite (Ghent *et al.*, 1987; Grambling, 1990). Temperature estimates

range from 508 °C, from amphibole-plagioclase thermometer to 521-523 ºC, obtained from Fe-Mg thermometer between resorbed garnet rim and chlorite (Table 7).

Using Al-in-amphibole barometer (Anderson & Smith, 1995) and assuming T = 520 ºC, we obtained consistent pressure of 0.48 GPa for M2 metamorphic event.

Average P-T estimates obtained from THERMOCALC are T = 575 ºC and P = 0.34 GPa (Table 8).

Our thermobaric investigations discussed above, constrains the peak high-pressure metamorphic conditions (M1 event) of P = 1.5-1.65 GPa and T = 447 - 580 ºC.

Assuming that the maximum pressure (1.6 GPa) recorded by the quartz schist is due exclusively to the lithostatic pressure, we estimated that the quartz schists from the Chadegan complex reached depths of at least 64 km, corresponding to a geothermal gradient of almost 7-8º C/km, that is clearly consistent with metamorphism in a subduction zone.

Thermobaric calculations show a nearly retrograde decompressive path from an amphibolite-eclogite- to amphibolite-facies conditions (Fig. 9). Garnet zoning with bell-shaped Mn and bowl-shaped Mg profile indicates that the overall shape of the P-T path is clockwise (Fig. 9) but the prograde path remains unconstrained.

As the M2 metamorphic assemblage occurred during the retrograde path, the D2 penetrative fabrics were acquired during the exhumation of the Chadegan complex. The exhumation of the Chadegan complex is probably contemporaneous with D2 shearing deformation.

Geodynamic Model

Our new structural and metamorphic data discussed above, coupled with other works carried out in different parts of the Sanandaj-Sirjan zone (Mohajjel *et al.*, 2003; Agard *et al.*, 2005; Agard *et al.*, 2006; Ghasemi & Talbot, 2006; Sheikholeslami *et al.*, 2008) allow us to suggest a geodynamic scenario which can explain the complex geological evolution recorded in the area during the rifting and the subsequent subduction and continental collision between Arabian and Iranian continental plates during Paleozoic up to Cenozoic (Fig. 10).

According to Berberian & King (1981), during the subduction of the Hercynian or Paleotethys oceanic crust at the northern part of Iran microplate, a new rift, localized approximately at the present location of the main Zagros thrust was generated. This rifting led to the formation of the Neotethys ocean and the movement towards north of the Iranian microplate.

From Permian to Triassic, two main stages of rifting have been suggested (Mohajjel *et al.*, 2003; Ghasemi & Talbot, 2006). The first stage started probably during Permian in the Zagros basin and was followed during Late Permian by wide basalt activity along the Sanandaj-Sirjan zone (Ghasemi & Talbot, 2006). The second rifting stage started during Triassic and has been well described in the north-western sector of the Sanandaj-Sirjan zone where Triassic continental and shallow marine sedimentary successions were interrupted by widespread basaltic magmatic activity with tholeitic affinity (Alavi & Mahdavi, 1994).

Triassic carbonates and basic lava documented in the Chadegan area and surroundings, testify extensional tectonic regime recorded during the second episode of rifting in the Sanandaj-Sirjan zone (Ghasemi *et al.*, 2005).

Jurassic metamorphism coupled with the magmatic activity documented along the southern sector of the Sanandaj-Sirjan zone, indicate that the subduction of Neotethyan oceanic crust beneath the south of Sanandaj-Sirjan zone may have already started during Late Jurassic-Cretaceous (Ghasemi & Talbot, 2006). However, geochemical studies on volcanic rocks in the ophiolitic complexes in the Zagros orogenic belt (Ghazi & Hassnipak, 1999b), indicate that most of them were generated in an intra-oceanic island arc environment, developed as consequence of the ocean-ocean subduction during Early-Middle Jurassic.

Intra-oceanic island arc in the Neotethys ocean was then obducted onto the northeastern margin of the Arabian plate (Ghasemi & Talbot, 2006) (Fig. 10).

According to Şengör & Natal'in (1996), subduction is a long-lived process that started from the Middle Jurassic and continued to the Early Miocene. Mohajjel *et al.* (2003) instead, suggested that the convergent regime developed for a longer period of time, spanning from Jurassic up to Cretaceous whereas Berberian & King (1981) studying igneous sequences adjacent to the northeastern Sanandaj-Sirjan zone suggested that the subduction process occurred during the Jurassic-Quaternary interval (Fig. 10).
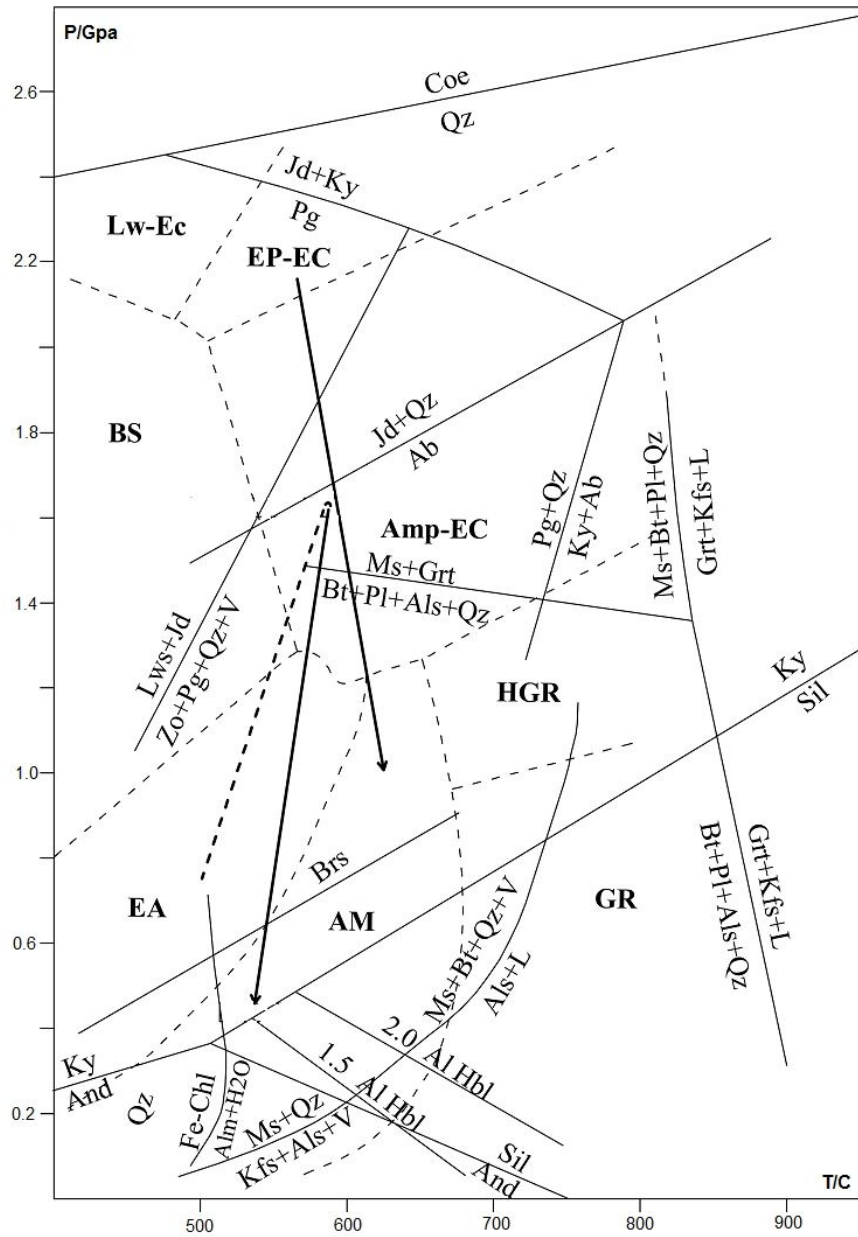
Figure 9: Petrogenetic gird and P-T paths for the metamorphic complex in the Chadegan metamorphic complex. Rectangles show P and T estimates obtained for M1 and M2 metamorphic events. The black arrows indicate P-T path for quartz schists. Dash light grey arrow indicates the estimated P-T path for the eclogite from north of Shahrekord (Davoudian *et al.,* 2008). Ab = Jd + Qtz after Holland (1980). Hornblende Al$_{tot}$ contents are after Plyusnina (1982). Aluminium silicate triple-point according to Holdaway (1971). Coesite = quartz curve after Bohlen & Boettcher (1982). Barroisite stability field after Ernst (1979). Reactions Ms + Qz = Kfs + Als + V and Ms + Bt + Qz + V = Als + L are after Vielzeuf & Holloway (1988). Reactions Ms + Grt = Bt + Pl + Als + Qz and Ms + Bt + Pl + Qz = Grt + Kfs + L and Bt + Pl + Als + Qz = Grt + Kfs + L are after Vielzeuf & Schmidt (2001). Reaction Jd + Ky = Pg and Pg + Qz = Ky + Ab from Holland (1979). Reaction Fe-Chl + Qz = Alm + H$_2$O after Hsu (1968). Reaction Lws + Jd = Zo + Pg + Qz + V from Heinrich & Althaus (1988). The background petrogenetic grid is from Ernst (2006). Metamorphic-facies abbreviations are: AM = amphibolite; Amp-EC = amphibolite-eclogite; BS = blueschist; EA = epidote amphibolite; Ep-EC = epidote-eclogite; GR = sillimanite-granulite; HGR = kyanite-granulite; Lw-EC = lawsonite-eclogite. Mineral abbreviations for names are from Whitney & Evans (2010).
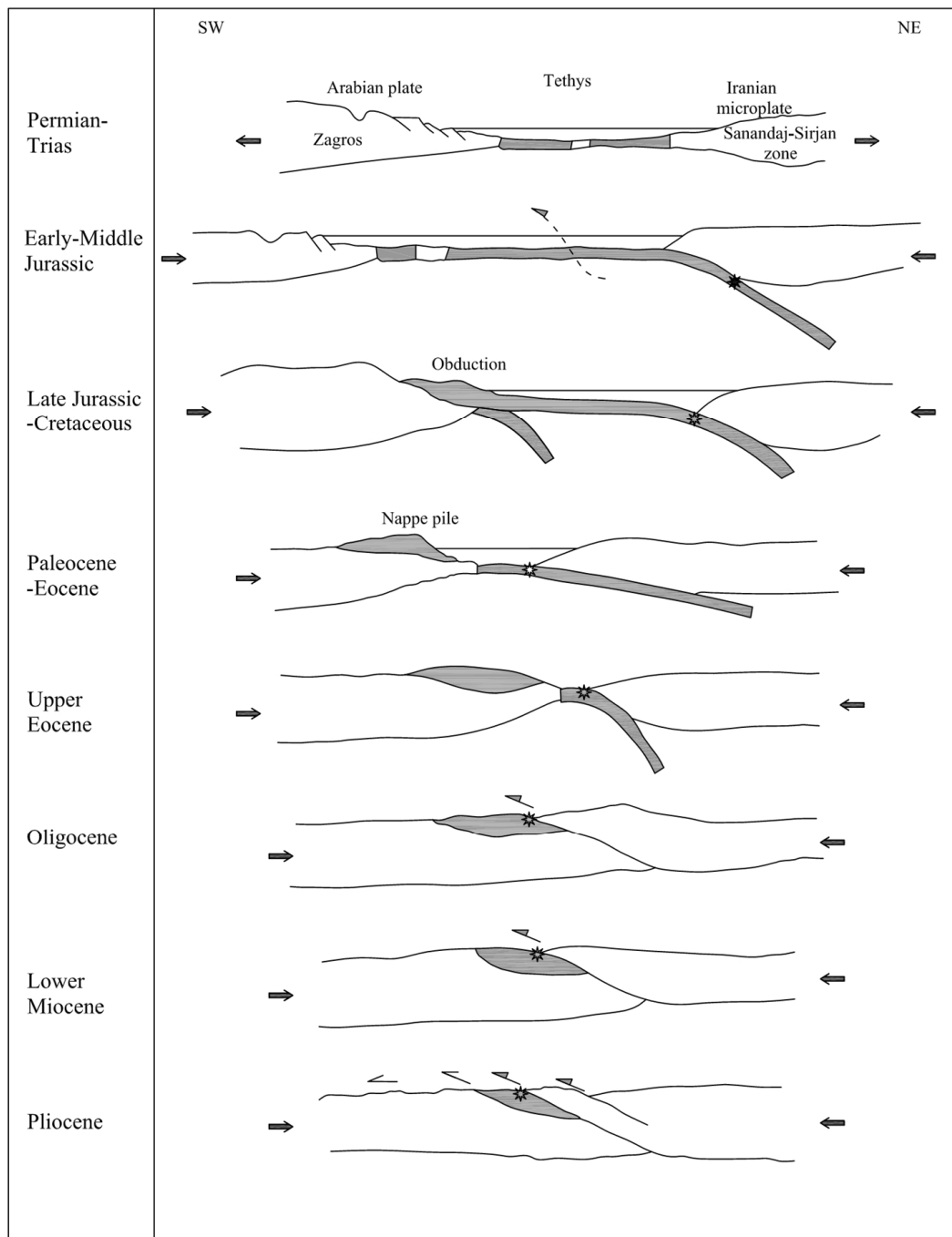
Figure 10: Hypothetic geodynamic evolution between Arabian and Iran continental margins deduced from our data and from literatures (modified after Agard *et al.*, 2005). Filled and open stars represent approximately the position of the subducted and exhumed Chadegan metamorphic complex respectively.

In this view, the high-pressure metamorphic conditions documented in the Chadegan metamorphic complex (M1 metamorphism – D1 deformation) can be interpreted as the result of the Neotethyan oceanic lithosphere subduction under the Iranian continental plate during the Early-Middle Jurassic.

The main event of ophiolitic obduction on the northeastern margin of the Arabian peninsula occurred during 100-70 Ma (Mohajjel *et al,* 2003; Agard *et al.,* 2005) (Fig. 10). On the basis of radiometric age carried out in the Zagros blueschists (Agard *et al.,* 2005), they inferred that the ophiolitic sequences in the Sanandaj-Sirjan zone were exhumed by a modification of the mechanical coupling between the upper and lower plate in response to obduction process. This exhumation process was short-lived and stopped at around 80

Ma, before the continental collision between the Arabia and Iran continental (Agard *et al.*, 2006).

Coupling tectono-metamorphic investigations and geochronological analyses, Sheikholeslamei *et al.* (2008) suggested that exhumation of the metamorphic rocks in the Neyriz metamorphic complex (located at the southeastern sector of the Sanandaj-Sirjan zone) have been occurred during Jurassic.

In the studied area, the Late Jurassic-Early Cretaceous sedimentary sequences deposited above the Chadegan complex metamorphic rocks, were neither deformed by D1 and D2 deformational phases nor were affected by M1 and M2 metamorphism. In detail, these unmetamorphosed sequences are made by sandstone, carbonate sequences, and by a basal conglomerate made from pebbles of metamorphic rocks similar to those belonging to the Chadegan metamorphic complex.

Therefore, the exhumation process was short-lived and finished before the end of Jurassic (Ghasemi *et al.*, 2005)(Fig. 10). The exhumation of the Chadegan metamorphic complex occurred through a decompressive and nearly isothermal path to the upper structural levels, where quartz schists recorded $P = 0.34 - 0.48$ GPa and $T = 508 - 575$ °C (M2 metamorphism - D2 deformation). This exhumation was due to the activation of the D2 shear belt probably in a transpressive regime.

Paleogeographic reconstruction of Neotethys, in fact, shows that Neothetys remained open along the Zagros suture untill Eocene or Miocene (Şengör & Natal'in, 1996). The timing of Neotethys closure along the Zagros suture, however remains a point of debate. Some authors suggest that the continental collision occurred during the Late Cretaceous (Berberian & King, 1981; Alavi, 1994) whereas alternative model suggests that the continental collision along the Zagros suture occurred during Miocene (Şengör & Natal'in, 1996; Agard *et al.*, 2005).

In the Chadegan area, the Paleocene-Eocene sedimentary successions were deformed by folds that show similar orientation and geometry to F3 folds documented in the Chadegan metamorphic complex. As a consequence, we suggest that these sedimentary successions have been deposited on the still active Iranian margin and that oceanic closure and continental collision must have taken during Oligocene-Miocene.

Conclusions

The most important results of our investigation are:

1- Quartz schists, cropping out at the limbs of the Chadegan metamorphic complex, record a polyphase tectono-metamorphic evolution. Relicts of D1 deformation phase are preserved as inclusion trails in the core of albite crystals whereas D2 deformation, the pervasive deformation of the area, produced a penetrative S2 axial plane foliation, a weakly and poor developed mylonitic foliation, F2 folds and L2 mineral lineation. D1 and D2 structures are themselves deformed by a post-Eocene deformation phase (D3) that produced S3 crenulation cleavage and F3 folds with NW-SE trending axis.

2- Two main metamorphism can be documented: (1) relicts of high-pressure metamorphic mineral assemblage (M1) such as phengite + garnet + sodic-calcic amphibole, has been documented along S1 foliation and preserved as inclusions in the core of albite, whereas a later amphibolite-facies metamorphism (M2) occurred during the D2 deformation phase. No metamorphic growth event has been documented during D3 deformation phase.

3- During the Early-Middle Jurassic, the Chadegan complex belonging to the southern margin of the Iranian plate was involved in an accretionary prism and recorded a maximum pressure of 1.65 GPa and temperature of 447 - 580 °C (M1 metamorphism - D1 deformation). After this high-pressure event, the activation of the D2 shear belt (probably during a transpressive regime) was responsible for exhumation of orthogneiss (+ eclogites) and quartz schists. The exhumation occurred through a decompressive and nearly isothermal path to the upper structural levels, where quartz schists recorded $P = 0.34 - 0.48$ GPa and $T = 508 - 575$ °C (M2 metamorphism – D2 deformation event) probably before the end of Cretaceous.

References

Agard, P., Omrani, J., Jolivet, L., Mouthereau, F., 2005. Convergence history across Zagros (Iran): constraints from collisional and earlier deformation. International Journal of Earth Sciences**, 94: 401-419.

Agard, P., Monié, P., Gerber, W., Omrani, J., Molinaro, M., Meyer, B., Laborousse, L., Vrielynck, B., Jolivet, L., Yamato, P., 2006. Transient, synobduction exhumation of Zagros blueschists inferred from P-T, deformation, time, and kinematic constraints: Implications for Neotethyan wedge dynamics. Journal of Geophysical Research, 111: 1-28.

Alavi, M., 1994. Tectonics of the Zagros orogenic belt of Iran: new data and interpretations. Tectonophysics, 229: 211-238.

Alavi, M., Mahdavi, M. A., 1994. Stratigraphy and structure of the Nahavand region in western Iran and their implications for the Zagros tectonics. Geological Magazine, 131: 43-47.

Anderson, J.L., Smith, D.R., 1995. The effects of temperature and oxygen fugacity on the Al-in-hornblende barometer. American Mineralogist, 80: 549-559.

Armstrong, J.T., 1988. Quantitative analysis of silicates and oxide minerals: Comparison of Monte-Carlo, ZAF and Phi-Rho-Z procedure. Microbeam Analysis, 239-246.

Berberian, M., 1977. Three phases of metamorphism in Haji-Abad quadrangle (southern extremity of Sanandaj-Sirjan structural zone): a palaeotectonic discussion. In: Berberian, M. (Ed.), Contribution to the seismotectonics of Iran (part 3). Geological Survey of Iran, Tehran, Iran, pp. 239-263.

Berberian, M., King, G.C., 1981. Towards a paleogeography and tectonics evolution of Iran. Canadian Journal of Earth Sciences, 18: 210-265.

Berberian, M., 1995. Master blind thrust faults hidden under the Zagros folds: active basement tectonics and surface morphotectonics. Tectonophysics, 241: 193-224.

Bohlen, S.R., Boettcher, A.L., 1982. The quartz-coesite transformation: a pressure determination and effects of other composition. Journal of Geophysical Research, 87: 7073-7078.

Carswell, D.A., Wilson, R.N., Zhai, M., 2000. Metamorphic evolution, mineral chemistry and thermobarometry of schists and orthogneisses hosting ultra-high pressure eclogites in the Dabieshan of central China. Lithos, 52: 121-156.

Dale, J., Holland, T.J.B., Powell, R., 2000. Hornblende-garnet-plagioclase-thermobarometry: a natural assemblage calibration of the thermodynamics of hornblende. Contributions to Mineralogy and Petrology, 40:353-362.

Davoudian, A.R., Genser, J., Dachs, E., Shabanian, N., 2008. Petrology of eclogite from north of Shahrekord, Sanandaj-Sirjan zone, Iran. Mineralogy and Petrology, 92: 393-413.

Deer, W.A., Howie, R.A., Zussman, J., 1992. An introduction to the rock-forming minerals. Second Edition, Longman Scientific and Technical, Harlow, England,.696 pp.

Ernst, W.G., 1979. Coexisting sodic-calcic amphiboles from high-pressure metamorphic belts and the stability of barroisitic amphiboles. Mineralogical Magazine, 43: 269-278.

Ernst, W.G., 2006. Preservation/exhumation of ultrahigh-pressure subduction complexes. Lithos, 92: 321-335.

Ghasemi, A., Haji Hosseini, A., Hosseini, M., 2005. Geological map of Chadegan, Geological Survey of Iran, scale 1:100000.

Ghasemi, A., Talbot, C., 2006. A new tectonic scenario for the Sanandaj-Sirjan Zone (Iran). Journal of Asian Earth Sciences, 26: 683-693.

Ghazi, A.M., Hassanipak, A.A., 1999b. Geochemistry of sub-alkaline and alkaline extrusive from Kermanshah ophiolite, Zagros suture zone, western Iran: implications for Tethyan plate tectonics. Journal of Asian Earth Sciences, 17: 319-332.

Ghent, E.D., Stout, M.Z., Black, P.M., Brothers, R.M., 1987. Chloritoid bearing rocks associated with blueschists and eclogites, northern New Caledonia. Journal of Metamorphic Geology, 5: 239-254.

Grambling, J. A., 1990. Internally-consistent geothermometry and H_2O barometry in metamorphic rocks: the example garnet-chlorite-quartz. Contributions to Mineralogy and Petrology, 105: 617-628.

Green, T.H., Hellman. P.l., 1982. Fe-Mg partitioning between coexisting garnet and phengite at high pressure and comments on a garnet-phengite geothermometer. Lithos, 15: 253-266.

Heinrich, H., Althaus, E., 1988. Experimental determination of the 4 lawsonite + albite = paragonite + 2 zoisite + 2 quartz + 6 H2O. Neues Jahrbuch für Mineralogie Monatshefte, 11: 516-528.

Holdaway, M.J., 1971. Stability of andalusite and the aluminium silicate phase diagram. American Journal of Science, 271: 97-131.

Holland, T.J.B., 1979. Experimental determination of the reaction paragonite=jadeite+kyanite+H_2O, and internally consistent thermodynamic data for part of the system Na_2O-Al_2O_3-SiO_2-H_2O, with applications to eclogites and blueschists. Contributions to Mineralogy and Petrology, 68: 293-301.

Holland, T.J.B., 1980. The reaction albite=jadeite+quartz determined experimentally in the range 600-1200°C. American Mineralogist, 65: 129-134.

Holland, T.J.B., Powell R., 1998. An internally consistent thermodynamic data set for phases of petrological interest. Journal of Metamorphic Geology, 16: 309-343.

Hsu, L.C., 1968. Selected phase relationships in the system Al-Mn-Si-O-H: a model for garnet equilibria. Journal of Petrology, 98: 40-83.

Krogh, E.J., Raheim, A., 1978. Temperature and pressure dependence of Fe-Mg partitioning between garnet and phengite with particular reference to eclogite. Contributions to Mineralogy and Petrology, 66: 75-80.

Leake, B.E., Woolley, A.R., Arps, C.E.S., Birch W.D., Gilbert M.C., Grice J.D., Hawthorne F.C., Kato, A., Kisch, H.J., Krivovichev, V.G., Linthout, K., Laird, J., Mandarino, J.M., Maresch, W.V., Nickel, E.H., Rock N.M.S., Schmacher, J.C., Smith, D.C., Stepehnson, N.C.N., Ungaretti, L., Whittaker, E.J.W., Youzhi, G., 1997. Nomenclature of amphiboles: Report of the subcommittee on Amphiboles of the International Mineralogical Association on New Minerals and Mineral Names. American Mineralogist, 82: 1019-1037.

Massonne, H.J., Schreyer, W., 1987. Phengite geobarometry based on the limiting assemblage with K-feldspar, phlogopite and quartz. Contributions to Mineralogy and Petrology, 96: 212-224.

Mohajjel, M., Fergusson, C.L., Sahandi, M.R., 2003. Cretaceous-Tertiary convergence and continental collision, Sanandaj-Sirjan Zone, western Iran. Journal of Asian Earth Sciences, 21: 397-412.

Palmieri, R., Ghiribelli, B., Talarico, F., Ricci, C.A., 2003. Ultra-high-pressure metamorphism in felsic rocks: the garnet-phengite gneisses and quartzites from the Lanterman Range, Antractica. European Journal of Mineralogy, 15: 513-525.

Powell, R., Holland, T.J.B., 1988. An internally consistent dataset with uncertainities and correlations: 3. Aplications to geobarometry, worked examples and a computer program. Journal of Metamorphic Geology, 6: 173-204.

Plyusnina, L.P., 1982. Geothermometry and geobarometry of plagioclase-hornblende-bearing assemblage. Contributions to Mineralogy and Petrology, 80: 140-146.

Ravna, E.K., 2000. The garnet-clinopyroxene Fe^{+2}-Mg geothermobarometer:an updated calibration. Journal of Metamorphic Geology, 18: 211-219.

Şengör, A.M.C., 1984. The cimmeride orogenic system and the tectonics of Eurasia. Geological Society of America Special Paper, 195.

Şengör, A.M.C. Natal'in, B.A., 1996. Paleotectonics of Asia: fragments of a synthesis. In: Yin, A., Harrison, T.M. (Eds.), The tectonics evolution of Asia. Cambridge University Press, pp. 486-640.

Sheikholeslami, M.R., Pique, A., Mobayen, P., Sabzehei, M., Bellon, H., Hashem Emami, M., 2008. Tectono-metamorphic evolution of the Neyriz metamorphic complex, Quri-Kor-e- Sefid area (Sanandaj-Sirjan Zone, SW Iran). Journal of Asian Earth Sciences, 31: 504-521.

Spear, F.S., 1991. On the interpretation of peak metamorphic temperature in light of garnet diffusion during cooling. Journal of Metamorphic Geology, 9: 379-388.

Stöclin, J., 1968. Structural history and tectonics of Iran: a review. American Association of Petroleum Geology Bulletin, 52: 1229-1258.

Vielzeuf, D., Holloway, J.R., 1988. Experimental determination of the fluid-absent melting relations in the pelitic system. Contributions to Mineralogy and Petrology, 98: 257-276.

Vielzeuf, D., Schmidt, M., 2001. Melting relations in hydrous system revisited: application to metapelites, metagreywackes and metabasalts. Contributions to Mineralogy and Petrology, 141: 251-267.

Vidal, O., Parra, T., 2000. Exhumation paths of high-pressure metapelites obtained from local equilibria for chlorite-phengite assemblage. Geological Journal, 35: 139-161.

Whitney, D.L., Evans, B.W., 2010. Abbreviations for names of rock-forming minerals. American Mineralogist, 95: 185-187.